SF2A 2014
J. Ballet, F. Bournaud, F. Martins, R. Monier and C. Reylé (eds)

LIDT-DD: A NEW HYBRID MODEL TO UNDERSTAND DEBRIS DISCS OBSERVATIONS - THE CASE OF MASSIVE COLLISIONS.

Q. Kral[1], P. Thébault[1], J.-C. Augereau[2], A. Boccaletti[1] and S. Charnoz[3]

Abstract. LIDT-DD is a new hybrid model coupling the collisional and dynamical evolution in debris discs in a self-consistent way. It has been developed in a way that allows to treat a large number of different astrophysical cases where collisions and dynamics have an important role. This interplay was often totally neglected in previous studies whereas, even for the simplest configurations, the real physics of debris discs imposes strong constraints and interactions between dynamics and collisions.

After presenting the LIDT-DD model, we will describe the evolution of violent stochastic collisional events with this model. These massive impacts have been invoked as a possible explanation for some debris discs displaying pronounced azimuthal asymmetries or having a luminosity excess exceeding that expected for systems at collisional steady-state. So far, no thorough modelling of the consequences of such stochastic events has been carried out, mainly because of the extreme numerical challenge of coupling the dynamical and collisional evolution of the released dust.

We follow the collisional and dynamical evolution of dust released after the breakup of a Ceres-sized body at 6 AU from its central star. We investigate the duration, magnitude and spatial structure of the signature left by such a violent event, as well as its observational detectability. We use the GRaTer package to estimate the system's luminosity at different wavelengths and derive synthetic images for the SPHERE/VLT and MIRI/JWST instruments.

Keywords: planetary system – debris discs – massive collisions – circumstellar matter

1 Introduction

The collisional breakup of large planetesimals has been invoked as a possible cause for some pronounced structures observed in resolved debris discs. It has also been considered as an explanation for some "anomalously" bright discs that are too old for their luminosity to be explained by a steady-state erosive collisional cascade (Wyatt 2008; Gáspár et al. 2013).

Although this important issue has been explored in some past numerical studies, these numerical models were limited by the absence of (or a very simplified) coupling between the collisional and dynamical evolutions of the post-breakup fragment cloud (Kenyon & Bromley 2004; Jackson & Wyatt 2012; Jackson et al. 2014).

We propose here to address this problem using the new generation LIDT-DD code, specifically developed for the coupled study of collisions and dynamics in debris discs (Kral et al. 2014). Our main objective is to estimate the observability and the longevity of the dust disc formed in the aftermath of such a violent and transient event. We focus especially on how the concurring effects of collisions and radiation pressure affect the asymmetric post-breakup structures.

2 The LIDT-DD model

For a full description of our code, we refer the reader to Kral et al. (2013). Let us here briefly summarize its main characteristics as well as the main important features that have been implemented so far.

[1] LESIA-Observatoire de Paris, UPMC Univ. Paris 06, Univ. Paris-Diderot, France
[2] Univ. Grenoble Alpes and CNRS, IPAG, F-38000 Grenoble, France
[3] Laboratoire AIM, Université Paris Diderot / CEA / CNRS, Institut Universitaire de France

The basic principle of the LIDT-DD model is to couple a Lagrangian approach for the dynamics to a particle-in-a-box statistical Eulerian one for the collisional evolution (Charnoz & Taillifet 2012). At a given location in the system, all particles of a given size *and* sharing similar dynamical characteristics are gathered into larger super-particles (called "tracers"), whose dynamical evolution is followed with an N-body scheme, while their collisional evolution is investigated with a statistical approach, considering all mutual tracer-tracer impacts at any given location in the system.

The procedure to evolve both the tracers' dynamics and collisions can be sketched as follows. Each particle in the code is a super-particle representing a vast population of same-sized physical particles. The positions and velocities of the tracers are integrated with a Bulirsh-Stöer scheme (N-body approach) that is able to include different type of forces (Poynting-Robertson drag, radiation pressure, gravitational interactions, gas drag if needed). Once the dynamics has been integrated over one time step, the system is divided into spatial cells. The collisional evolution is then estimated cell by cell, by taking into account all potential tracer-tracer encounters within each cell. Although LIDT-DD is intrinsically 3-D and tracers dynamics is integrated in the vertical direction, we use a 2-D grid (r,θ) for these "collisional cells", each individual cell having a finite vertical extension equal to the tracers' inclination times the radial distance. All tracer-tracer collisions are then treated with a statistical procedure, taking into account the mutual velocities between tracers and the number density of real physical particles they represent. The size-distribution of the fragments produced by each of these impacts is estimated with the collisional outcome prescription used in the statistical code of Thebault & Augereau (2007). Its main parameter is the critical specific energy Q^* required for dispersing at least 50% of the target. Both fragmenting ($Q > Q^*$, where Q is the collision kinetic energy per target unit mass), and cratering (or "erosive", $Q < Q^*$) impacts are taken into account. The collisional debris are then redistributed, according to their sizes and dynamical characteristics, into newly-created tracers. The feedback of collisions onto the old and new tracers (momentum redistribution and energy loss) is taken into account. After each time step, tracers of a given spatial cell are sorted into dynamical "families", in order not to lose important information about the dynamical complexity of the system (for instance, at a given location, grains having similar sizes can have different origins and thus different dynamical evolutions). Eventually, to avoid an unmanageable increase of the number of tracers, the code is looking, at the end of each time step, for redundant tracers which are then merged into the nearest tracers representing the same size and dynamical family.

3 Massive collisions

For a full description of our results, we refer the reader to Kral et al. (2014). Here we recall the setup and give the most important results found by our study.

3.1 Setup

We follow the evolution of a massive amount of small fragments, of mass $M_{\rm frag} = 10^{21}$ kg, released by a violent phenomenon, in the inner regions (at $r_{\rm init} = 6\,$AU) of a planetary system around an A7V star. If we assume that $M_{\rm frag}$ corresponds to the mass of the object that has been shattered, then this object's radius is $\sim 500\,$km, approximately the size of Ceres.

Given that the breakup of such a large object requires an impact with a massive projectile, and that the probability for such two-body encounters is likely to decrease with object sizes, we consider here that $v_{\rm frag}$, the velocities of the escaping post-impact fragments, are randomly distributed between 0 and $v_{\rm esc}$, where $v_{\rm esc}$ is the escape velocity of the initial target. The initial velocity has then two components: 1) the Keplerian velocity of the progenitor parent body, and 2) a kick velocity, which has no reasons not to be isotropic (Jackson & Wyatt 2012), where kick angles are isotropically distributed onto a sphere. The initial eccentricity and inclination distributions of the ejecta are then automatically obtained from this constraint on $v_{\rm frag}$. For our nominal set-up, we obtain $< e >= 2 < i >\sim 0.037$.

For the grain composition, crucial for the calculation of collision outcomes and for estimating their response to radiation pressure (value of β), but also for the production of synthetic images and SEDs with GRaTer, we consider generic astrosilicates (Draine 2003). For estimating observed luminosities, we consider that the star+disc system is at a distance of 30 pc.

The differential size distribution of the initial fragments follows a steep power law in $dN/ds \propto s^{-3.8}$, corresponding to the crushing law expected for the outcome of violent collisions (Takasawa et al. 2011; Leinhardt & Stewart 2012). The minimum size is taken to be around the blow-out size $s_{\rm cut}$ induced by radiation pressure,

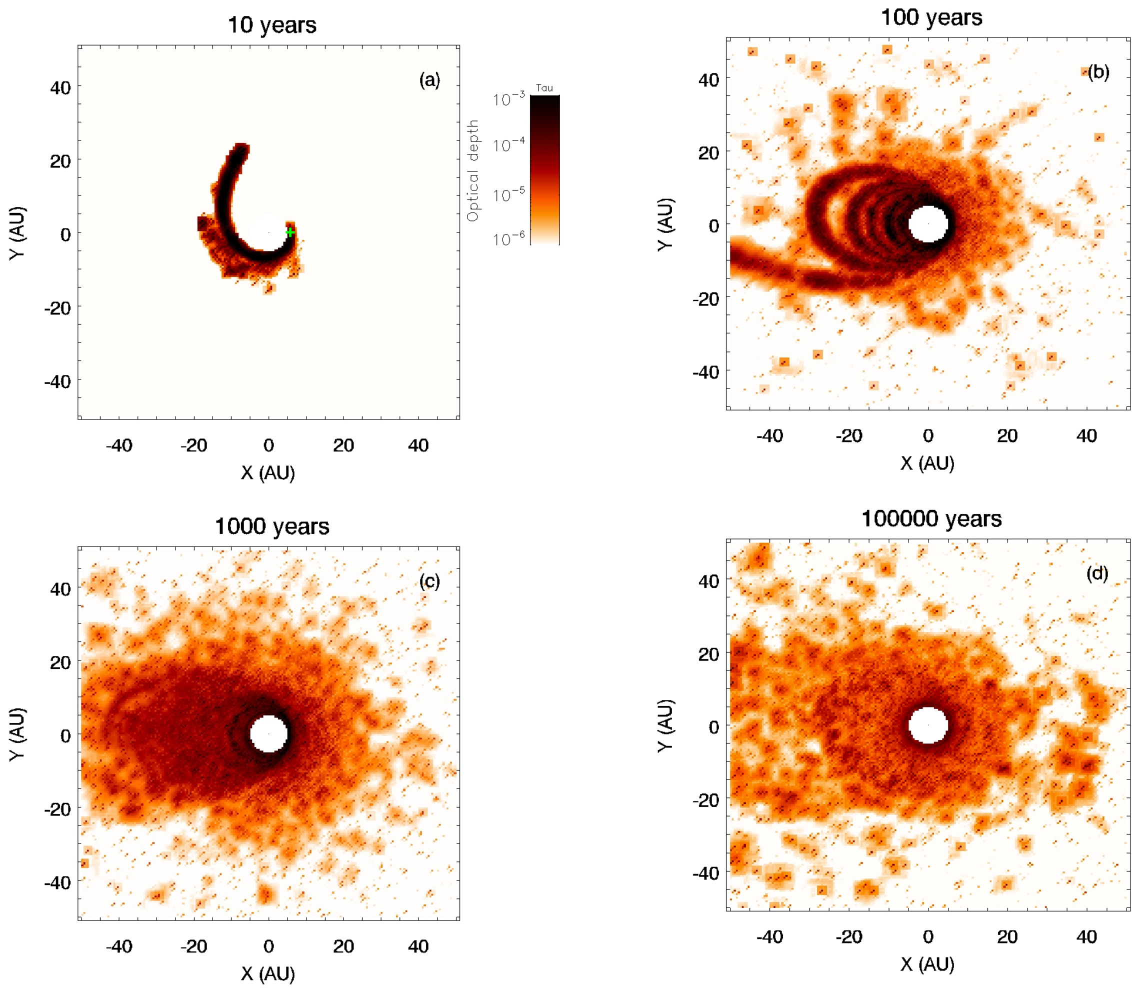

Fig. 1. Evolution of the system after the release of 10^{21}kg of material at 6 AU from the central A7V star. 2-D map of the optical depth at different epochs after the initial breakup. The green cross on plot (a) is the location of the initial breakup.

i.e., $\simeq 1.8\mu$m for compact astrosilicates around an A7V star. The maximum size of the initial fragments is set at 1m.

3.2 Results

3.2.1 Spatial Signature

In the immediate aftermath of the initial breakup, a one-armed spiral forms and propagates outwards (Fig. 1a). This spiral corresponds to the peak luminosity of the system's post-breakup evolution (see Fig. 2). Its outer parts consist mostly of small grains close to the blowout size, which are placed on highly-eccentric orbits by radiation pressure. The spiral fades out quickly and morphs into elongated concentric "ripples", which become more and more tightly wound with time (Fig. 1b). These features arise because all released fragments' orbits have to pass through the initial release position at X=6 AU, Y=0. As time goes by, however, these ripple features fade away and become undetectable after ~ 1000 years.

Next, the system enters a more long-lived phase where it assumes the shape of an asymmetric eccentric disc (Fig. 1c). This elongated shape is due to the fact that, during this period, most grains still have their orbits passing by a point close to the initial release location, and that the disc's geometrical cross section is dominated by small grains, close to the blowout limit, which have high-e orbits. Note, however, that the bulk of the system's *mass*, which is contained in the biggest particles, is located in a nearly-circular ring passing by the release point at 6 AU. This ring forms due to Keplerian shear over a few dynamical periods. Its width is set by the initial velocity dispersion of the post-release fragments. This ring logically also corresponds to the region where most of the collisional activity takes place. Hence, another brightness asymmetry created by the clustering of orbits close to the release point is clearly seen during the early evolution phase (Fig. 1c).

As time goes by, however, the asymmetric elongated disc structure progressively fades out. Figs 1c,d clearly show that the initially tenuous outer regions of the right-hand side progressively fill up with matter. This matter consists mostly of small grains, placed on high-e orbits by radiation pressure, which have been produced by second (or more) generation collisions in regions that are no longer that of the initial breakup. One of the main production sources is the aforementioned inner ring made of all the biggest initially released fragments.

3.2.2 Detectability

In order to estimate the detectability of this flux excess, we plot on Fig. 2 (left) the evolution of the disc-integrated flux at 24μm, as observed at a 30pc distance. As a typical criterion for detectability, we take as a reference the performance of the Spitzer/MIPS instrument at 24 microns. We consider that the disc-to-star flux ratio should exceed 10% for a 3 sigma, or larger, detection of an excess above the stellar photosphere.

As can be seen, for our nominal case, the disc signature remains detectable, at 24μm, for the whole duration of the simulation (10^5 years). Since $F_{\rm dust}/F_{\rm star}$ follows an approximate $t^{-0.3}$ decrease, it is easy to extrapolate the Fig. 2 (left) curve to later times. The extrapolated time at which the system reaches the critical $F_{\rm dust}/F_{\rm star} \sim 0.1$ value is then $\sim 10^6$ years, which gives the approximate duration of the detectability phase.

Another important result is that, in the inner disc regions ($\sim$ 6 AU) considered here, the flux excess due to one massive impact greatly exceeds that of a debris disc at steady-state, i.e., a disc whose luminosity is due to a "standard" collisional cascade. We verify this by plotting in Fig. 2 (left) the maximum possible luminosity (in black), at 2 different ages (1 and 10 Myrs after the equilibrium collisional cascade phase is reached), expected for such a steady-state disc. As can be clearly seen, our post massive-breakup disc is, for the whole duration of the simulation, at least one order of magnitude brighter than even a very young steady-state disc only 1 Myrs after its collisional cascade phase has begun.

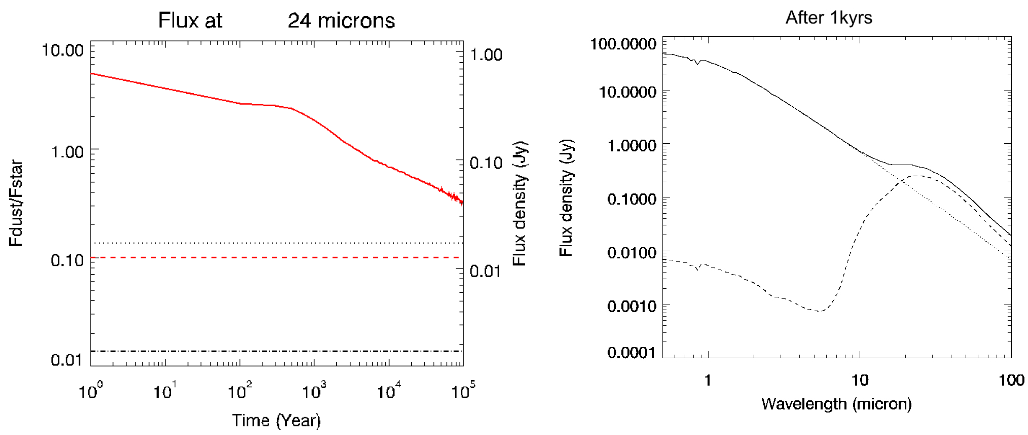

Fig. 2. Left : Evolution of the disc-integrated flux at 24 μm (red solid line). The red dashed line marks a dust-to-star flux ratio equal to 0.1, taken as our detectability criteria. The dotted and dash-dotted black lines give the maximum possible luminosity, at 1Myrs and 10Myrs, for a hypothetical collisional cascade at steady-state. The X-axis indicates the time after the breakup in years. The right-hand side Y-axis indicates the absolute flux in Jy, while the left-hand side axis displays the ratio of the disc flux to that of the stellar photosphere. **Right** : SED of the integrated system at 1 kyrs after the breakup. The full line represents the total (stellar photosphere + disc) luminosity, while the dashed line represents the sole contribution of the dust disc and the dotted one is that of the stellar photosphere.

Fig. 2 (right) shows the star+disc integrated SED, at 1kyrs after breakup, as computed with the GRaTer package. The excess due to the post-breakup dust appears clearly in the mid-IR domain, peaking around 25μm. This is confirmed by the synthetic images obtained with the GRaTer package at different wavelengths, showing that the dust disc is at its brightest in this $\lambda \sim 25\mu$m domain (see Fig. 3).

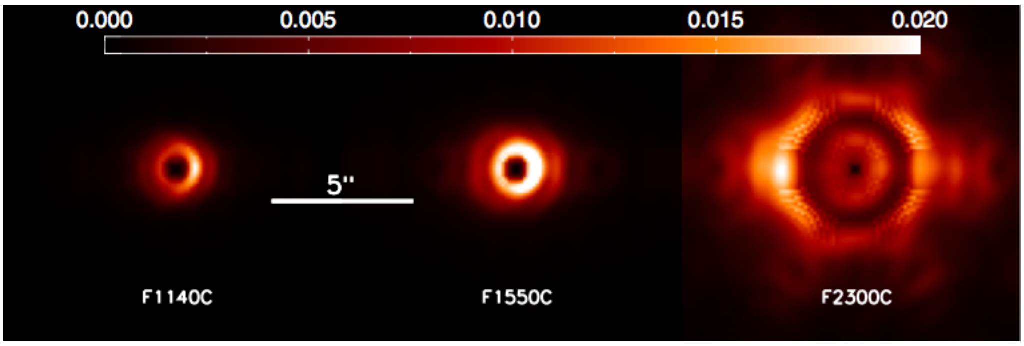

Fig. 3. Synthetic images, for the system in its "asymmetric disc" phase (at 10^4 years), at 10 pc, with the MIRI/JWST instrument with different filters at 11.4, 15.5 and 23μm (from left to right) obtained with the reference star subtraction method. The color scale gives the flux ratio with respect to the brightest pixel in the PSF (Point Spread Function).

We decided to go one step further and test the observability of the collision-induced discs with the expected performance of two instruments: SPHERE, at the VLT (Beuzit et al. 2008), and MIRI, the mid-IR instrument of JWST (Wright et al. 2010). We here compare the intensity level of the synthetic disc images to the residual starlight after processing the data, determined from simulations. Details about the procedure to create the synthetic images for each instrument are given in Kral et al. (2014).

The synthetic image with SPHERE (not shown here) at 1.6μm shows the potential to detect a left/right asymmetry in the inner region after a massive breakup happening at 10 pc, but the outer regions of the disc are undetectable.

Fig. 3 shows what would be seen by MIRI in thermal emission in the aftermath of such a collision. The 11.4μm image at 10 pc is relatively similar to the one obtained with the SPHERE simulation. It mainly shows the inner ring at the release distance (6 AU) and clearly reveals the increased luminosity of the right-hand side (the collision point) as compared to the left one. The situation is basically the same at 15.5μm, except that the image is brighter, which is logical because we are here closer to the wavelength at which the disc luminosity peaks. The disc brightness is such that even a system 500 times fainter would still be above the detectability limit. The peak luminosity is reached on the 23μm image, but the 2$''$ Lyot coronagraph does here occult a large part of the disc. The central shadowed region reduces to 20 AU, so that the external regions of the post-breakup disc become visible. Interestingly, the brightest side of the disc is now the left region. This is a logical result, because this left outer region is mostly populated by small grains collisionally produced in the dense right-hand-side ansae of the ring and placed on eccentric orbits by radiation pressure.

We conclude that multi-wavelength observations with SPHERE, and above all MIRI, have the potential to resolve the signature of massive collisional events in the inner regions of nearby debris discs.

4 Conclusions

We presented the principle of the new LIDT-DD model and we have shown its potential on a first astrophysical case, that of massive collisions in an otherwise dust-empty region. This configuration had already been investigated in some previous studies, but so far only with simplified collisional and/or dynamical prescriptions (Lisse et al. 2009; Jackson & Wyatt 2012; Johnson et al. 2012; Jackson et al. 2014). LIDT-DD allows us to relax most of these restrictive assumptions by self-consistently following the collisional and dynamical fate of the breakup fragments.

Our simulations have shown (Kral et al. 2014) that the breakup of a Ceres-sized body at 6 AU from an A star leads to a luminosity excess that greatly exceeds that of a standard disc at collisional steady-state. The breakup's aftermath can be decomposed into three distinct phases. Firstly, a bright spiral, composed of close-to $\beta = 0.5$ grains, quickly forms and evolves into ripple-like structures over a few dynamical timescales. In parallel, a narrow ring, made of the largest breakup fragments, forms by Keplerian shear at the radial location of the release. The second phase, which is more long-lived, corresponds to an asymmetric disc, brighter and more compact on the side of the initial breakup and more extended and diffuse on the opposite side. The luminosity of this disc decreases with time, while its asymmetries are progressively resorbed by collisional activity. The third and final phase corresponds to the symmetrization of the system, which occurs on a timescale of a few 10^5 years. An important point is that asymmetries are here resorbed by collisional activity *alone*, in the absence of planets or any other perturbing bodies or processes. More specifically, they are resorbed by the gradual dispersion of material due to the coupled effect of successive collisions and Keplerian motion, and the reprocessing of new fragments in regions initially devoid of material.

Using the GRaTer package, we find that the flux excess created by the initial breakup should be clearly detectable, at 24 μm, for the reference case of a Ceres mass body at 6 AU from an A7V star. This luminosity excess should be observable in photometry, at 30 pc, for at least $\sim 10^6$ years with Spitzer/MIPS.

To assess the observability of the asymmetries, we compute synthetic images for the SPHERE/VLT and MIRI/JWST instruments. With SPHERE at 1.6μm, the left/right asymmetry at the collision point (6 AU) should be detectable from a 10 pc distance, but just above the detection limit. The situation is more favourable with MIRI, as the same asymmetry should be clearly seen, at 10 pc, well above the detection limit at 11.4 and 15.5μm. At 23μm, because of the large Lyot coronagraph, only the external regions of the disc can be mapped out, but the left/right asymmetry is here also detected, albeit with the anti-breakup side now being the brightest. This is an expected result and could be used as an indicator of the signature of massive collisional events.

The present study has shown the potential of the LIDT-DD code for future investigations of massive collisions, in particular when coupled to the GRaTer package to produce accurate SEDs and synthetic images.

Q.K. acknowledges financial support from the French National Research Agency (ANR) through contract ANR-2010 BLAN-0505-01 (EXOZODI). SC acknowledges the financial support of the UnivEarthS Labex program at Sorbonne Paris Cit (ANR-10-LABX-0023 and ANR-11-IDEX-0005-02).

References

Beuzit, J.-L., Feldt, M., Dohlen, K., et al. 2008, Proc. SPIE, 7014,

Charnoz, S., Taillifet, E., 2012, ApJ, 753, 119

Draine, B. T. 2003, ARA&A, 41, 241

Gáspár, A., Rieke, G. H., & Balog, Z. 2013, ApJ, 768, 25

Jackson, A. P., & Wyatt, M. C. 2012, MNRAS, 425, 657

Jackson, A. P., Wyatt, M. C., Bonsor, A., & Veras, D. 2014, MNRAS, 440, 3757

Johnson, B. C., Lisse, C. M., Chen, C. H., et al. 2012, ApJ, 761, 45

Kenyon, S. J., & Bromley, B. C. 2004, AJ, 127, 513

Kral, Q.; Thebault, P.; Charnoz, S., 2013, A&A, 558, A121

Kral, Q., Thebault, P., Augereau, J.-C., Boccaletti, A., & Charnoz, S. 2014, arXiv:1409.7609

Leinhardt, Z. M., & Stewart, S. T. 2012, ApJ, 745, 79

Lisse, C. M., Chen, C. H., Wyatt, M. C., et al. 2009, ApJ, 701, 2019

Takasawa, S., Nakamura, A. M., Kadono, T., et al. 2011, ApJL, 733, L39

Thebault, P., Augereau, J. C., 2007, A&A, 472, 169

Wright, G. S., Rieke, G., Boeker, T., et al. 2010, Proc. SPIE, 7731,

Wyatt, M. C. 2008, ARA&A, 46, 339